Geophys. J. Int. (2008) **174,** 21–28 doi: 10.1111/j.1365-246X.2008.03829.x

Interpolation using a generalized Green's function for a spherical surface spline in tension

P. Wessel and J. M. Becker

Department of Geology & Geophysics, University of Hawaii, 1680 *East-West Rd, Honolulu,* HI 96822, *USA. E-mail: pwessel@hawaii.edu*

Accepted 2008 April 17. Received 2008 April 10; in original form 2008 February 12

SUMMARY

A variety of methods exist for interpolating Cartesian or spherical surface data onto an equidistant lattice in a procedure known as gridding. Methods based on Green's functions are particularly simple to implement. In such methods, the Green's function for the gridding operator is determined and the resulting gridding solution is composed of the superposition of contributions from each data constraint, weighted by the Green's function evaluated for all output–input point separations. The Green's function method allows for considerable flexibility, such as complete freedom in specifying where the solution will be evaluated (it does not have to be on a lattice) and the ability to include both surface heights and surface gradients as data constraints. Green's function solutions for Cartesian data in 1-, 2- and 3-D spaces are well known, as is the dilogarithm solution for minimum curvature spline on a spherical surface. Here, the spherical surface case is extended to include tension and the new generalized Green's function is derived. It is shown that the new function reduces to the dilogarithm solution in the limit of zero tension. Properties of the new function are examined and the new gridding method is implemented in Matlab® and demonstrated on three geophysical data sets.

Key words: Numerical solutions; Spatial analysis.

1 INTRODUCTION

Earth scientists often collect data that are not equidistantly sampled. As many processing and mapping procedures require such rigidly organized data (e.g. spectral analysis), a common data manipulation step involves resampling the data onto an equidistant grid; this process is commonly called gridding. There are numerous ways to accomplish gridding, including convolution-type filtering (Wegman & Wright 1983), kriging (e.g. Olea 1974; Omre & Halvorsen 1989; Reguzzoni *et al.* 2005), the projection onto convex sets (e.g. Menke 1991) and in particular splines (e.g. Briggs 1974; Freeden 1984; Inoue 1986; Sandwell 1987; Smith & Wessel 1990; Wahba 1990; Mitášová & Mitáš 1993). The latter technique is known to yield smooth solutions and has become very popular as much geoscience data are inherently smooth (e.g. geopotential fields). The smoothness of a surface f is assured by minimizing

$$E = \int_{S^2} (\nabla^2 f)^2 \, \mathrm{d}S, \tag{1}$$

the integrated squared curvature over the unit sphere S^2, yielding the familiar minimum curvature spline solution. However, when the constraining data are noisy or do not reflect a smooth underlying phenomenon (e.g. topographic relief) it then has proven advantageous to suppress unwanted oscillations in the solution by introducing tension (e.g. Smith & Wessel 1990). The main effect of tension is to counteract the tendency of splines to oscillate away from data constraints.

Most gridding techniques operate on an equidistant grid and solve the equations governing the gridding process with either finite difference or finite element implementations (e.g. Swain 1976; Renka 1984; Smith & Wessel 1990). An alternative approach, however, is to determine the Green's function for the gridding operator and to construct the solution as a sum of contributions from each data point, weighted by the Green's function evaluated for each point separation. The main benefit of this approach lies in (i) the simplicity of implementation, (ii) the ability to use surface gradients as data constraints and (iii) the freedom to choose any desirable configuration of input and output coordinates (not necessarily equidistant). For instance, Sandwell (1987) showed that minimum curvature gridding for Cartesian data in 1-, 2- and 3-D could be formulated via Green's functions, including the ability to incorporate gradient data in finding the surface solution. This method has been extended to include tension as well (e.g. Mitášová & Mitáš 1993; Wessel & Bercovici 1998).

For data collected over large portions of the Earth's surface, or for areas close to the polar regions, it is preferable to consider the data on a spherical rather than a planar surface. Gridding spherical data may be accomplished in a similar manner, using finite element implementations such as SSRFPACK (Renka 1997). For a minimum curvature solution, Parker (1994) showed that a Green's function could be determined, thus allowing this approach to be used with

spherical data as well. In this paper, we extend Parker's (1994) spherical method to include tension and determine the Green's function for continuous curvature splines in tension on a sphere. This new Green's function allows us to rapidly implement spherical gridding with tension for situations which may include a mix of surface and gradient data constraints.

2 SPHERICAL SURFACE SPLINE IN TENSION

By analogy with Cartesian cases (e.g. Wessel & Bercovici 1998), the interpolating function $f(\mathbf{x})$ must satisfy

$$\nabla_s^2 \left[\nabla_s^2 - p^2\right] f(\mathbf{x}) = \Phi(\mathbf{x}), \tag{2}$$

where p^2 is the (positive) tension constant, Φ is the source term, $\mathbf{x}$ (a unit radius vector) is a location on the sphere and ∇_s^2 is the spherical surface Laplacian,

$$\nabla_s^2 = \frac{1}{\sin\theta}\frac{\partial}{\partial\theta}\sin\theta\frac{\partial}{\partial\theta} + \cot\theta\frac{\partial}{\partial\theta} + \frac{1}{\sin^2\theta}\frac{\partial^2}{\partial\phi^2}, \tag{3}$$

where θ is colatitude and ϕ is longitude. The source term may be expressed as

$$\Phi(\mathbf{x}) = \sum_{j=1}^{N} \alpha_j \delta^{(2)}(\mathbf{x} - \mathbf{x}_j), \tag{4}$$

where $\mathbf{x}_j$ are the locations of the N data constraints, α_j are unknown coefficients and $\delta^{(2)}$ is the Dirac delta function on the spherical surface. The solution to (2) may then be specified (e.g. Sandwell 1987) as

$$f(\mathbf{x}) = \sum_{j=1}^{N} \alpha_j g_p(\mathbf{x}, \mathbf{x}_j), \tag{5}$$

where the Green's function $g_p(\mathbf{x}, \mathbf{x}')$ satisfies

$$\nabla_s^2 \left[\nabla_s^2 - p^2\right] g_p(\mathbf{x}, \mathbf{x}') = \delta^{(2)}(\mathbf{x} - \mathbf{x}'). \tag{6}$$

We seek $g_p(\mathbf{x}, \mathbf{x}')$ as an eigenfunction expansion of the fully normalized surface spherical harmonics

$$\nabla_s^2 Y_{lm}(\mathbf{x}) = -l(l+1)Y_{lm}(\mathbf{x}) \quad l = 0, 1, 2 \ldots \tag{7}$$

As $l = 0$ is an eigenvalue of (7), the Green's function defined in (6) does not exist. It is necessary to define the generalized Green's function (e.g. Courant & Hilbert 1953; Greenberg 1971; Roach 1982; Duffy 2001; Szmytkowski 2006), according to

$$\nabla_s^2 \left[\nabla_s^2 - p^2\right] \bar{g}_p(\mathbf{x}, \mathbf{x}') = \delta^{(2)}(\mathbf{x} - \mathbf{x}') - Y_{00}(\mathbf{x})Y_{00}^*(\mathbf{x}'), \tag{8}$$

where $\bar{g}_p(\mathbf{x}, \mathbf{x}')$ is orthogonal to the null space of (7)

$$\oint_{S^2} Y_{00}^*(\mathbf{x})\bar{g}_p(\mathbf{x}, \mathbf{x}')\,\mathrm{d}S = 0, \tag{9}$$

and the integral in (9) is taken over the surface of the unit sphere. Here, $Y_{00} = \frac{1}{\sqrt{4\pi}}$ is a constant, hence $\bar{g}_p(\mathbf{x}, \mathbf{x}')$ has zero mean. When the source term (4) also is orthogonal to the null space of (7), the interpolating function $f(\mathbf{x})$ may be expressed by

$$f(\mathbf{x}) = \beta Y_{00}(\mathbf{x}) + \sum_{j=1}^{N} \alpha_j \bar{g}_p(\mathbf{x}, \mathbf{x}_j), \tag{10}$$

where β is an arbitrary constant. The leading constant in (10) represents the part of the solution that maps into the null space of the gridding operator. We equate it with the mean data value $\bar{z}$ (i.e. $\beta = \sqrt{4\pi}\bar{z}$) and use data deviations $\Delta z_j = z_j - \bar{z}$ to constrain the remaining coefficients α_j by solving the square linear system (e.g. Sandwell 1987)

$$\Delta z_i = \sum_{j=1}^{N} \alpha_j \bar{g}_p(\mathbf{x}_i, \mathbf{x}_j), i = 1, N. \tag{11}$$

Following Wessel & Bercovici (1998) we introduce

$$\bar{c}_p(\mathbf{x}, \mathbf{x}') = \nabla_s^2 \bar{g}_p(\mathbf{x}, \mathbf{x}'), \tag{12}$$

the surface Laplacian of the generalized Green's function (here called 'curvature'), which then must satisfy the modified scalar Helmholtz equation,

$$\left[\nabla_s^2 - p^2\right] \bar{c}_p(\mathbf{x}, \mathbf{x}') = \delta^{(2)}(\mathbf{x}, \mathbf{x}') - Y_{00}(\mathbf{x})Y_{00}^*(\mathbf{x}'). \tag{13}$$

Substituting into (13) the spectral series expansions for $\bar{c}_p$ and $\delta^{(2)}$, and writing

$$Y_{00}(\mathbf{x})Y_{00}^*(\mathbf{x}') = \sum_{\ell=0}^{\infty}\sum_{m=-\ell}^{+\ell} \delta_{\ell 0} Y_{\ell m}(\mathbf{x})Y_{\ell m}^*(\mathbf{x}'), \tag{14}$$

where $\delta_{\ell m}$ is the Kronecker delta, we obtain the spectral series solution

$$\bar{c}_p(\mathbf{x}, \mathbf{x}') = -\sum_{\ell=1}^{\infty}\sum_{m=-\ell}^{+\ell} \frac{Y_{\ell m}(\mathbf{x})Y_{\ell m}^*(\mathbf{x}')}{\ell(\ell+1) + p^2}. \tag{15}$$

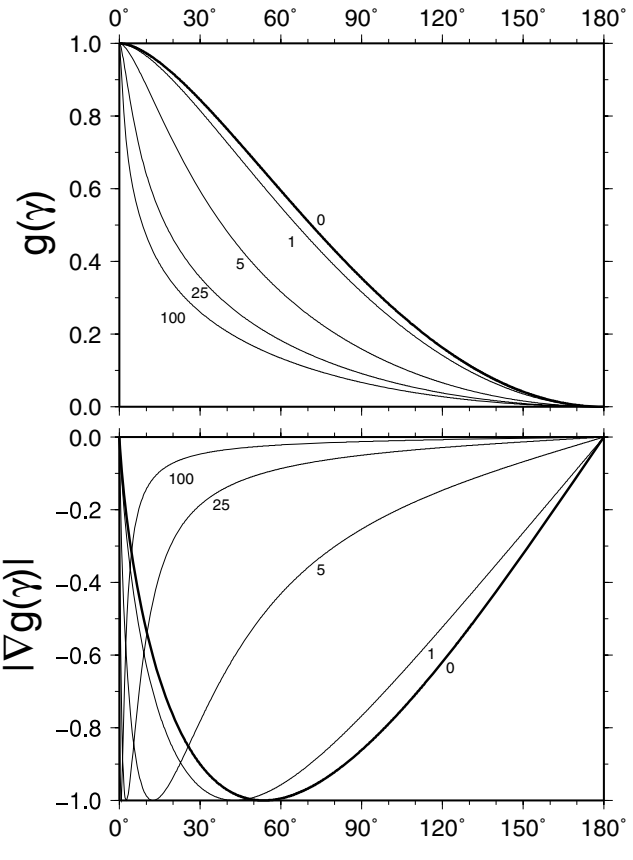

Figure 1. (Top panel) Green's function for spherical surface splines in tension for a range of tensions (labelled). The minimum curvature solution ($p = 0$) is drawn with a bold line. (Bottom panel) Norm of the gradient of the Green's function. Again, the bold curve corresponds to no tension. All curves have been normalized to a unit range.

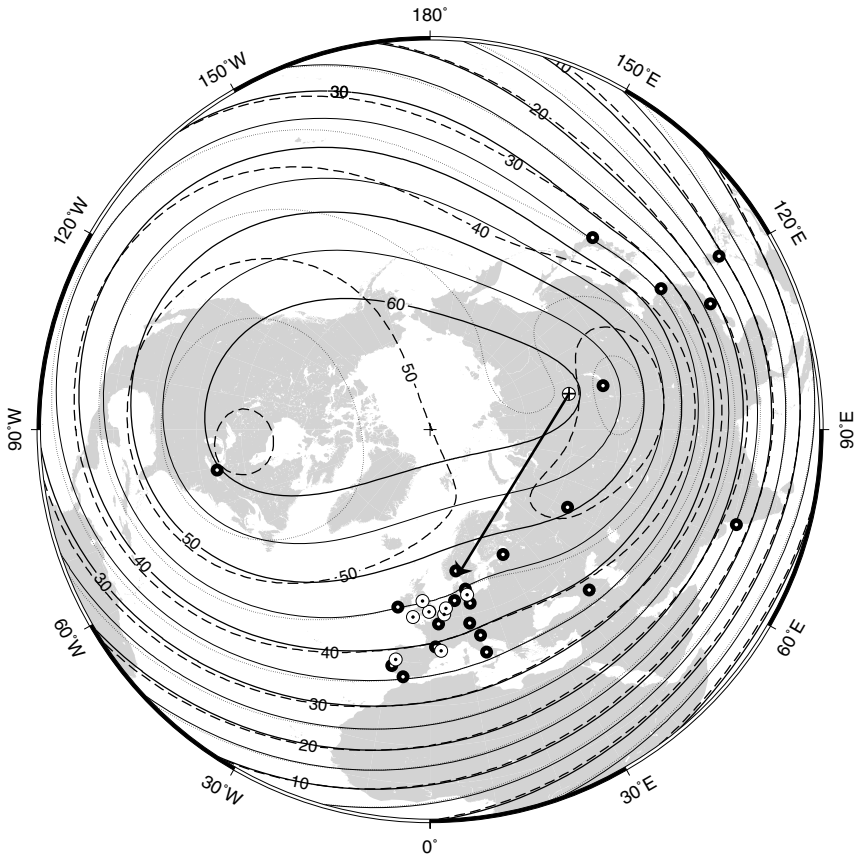

Figure 2. Contours (in μT) of the grids derived by Parker's (1994) dilogarithm solution with no tension for the northern hemisphere, based on 25 data constrains (solid black circles). Dashed and dotted contours represent the solution given in Parker (1994) where the incorrect point location for Oslo (crossed circle) was used. Solid contours represent solution using correct location (see arrow). Eight additional points (white circles) are used to validate the solution.

which does not include the $\ell = 0$ term. Using the Addition Theorem for spherical harmonics (e.g. Arfken & Weber 1995) to simplify the sum over m in (15), we obtain

$$\bar{c}_p(\mathbf{x}, \mathbf{x}') = \bar{c}_p(\cos\gamma) = \bar{c}_p(\gamma) = -\frac{1}{4\pi}\sum_{\ell=1}^{\infty}\frac{2\ell+1}{\ell(\ell+1)+p^2}P_\ell(\cos\gamma), \tag{16}$$

where γ is the angle between the two unit vectors $\mathbf{x}$ and $\mathbf{x}'$ and $P_\ell(\cos\gamma)$ is the Legendre polynomial of degree ℓ.

Gradshteyn & Ryzhik (1980, eq. 8.831.4) formulate the identity

$$\sum_{\ell=0}^{\infty}(-1)^\ell\left(\frac{1}{\nu-\ell}-\frac{1}{\nu+\ell+1}\right)P_\ell(\cos\phi) = \frac{\pi}{\sin\nu\pi}P_\nu(\cos\phi), \tag{17}$$

where P_ν is the associated Legendre function of the 1st kind. By letting $\cos\phi = -\cos\gamma$ and using the argument reflection formula $P_\ell(-x) = (-1)^\ell P_\ell(x)$ we rewrite (17) as

$$\sum_{\ell=0}^{\infty}\frac{2\ell+1}{\ell(\ell+1)-\nu(\nu+1)}P_\ell(\cos\gamma) = -\frac{\pi}{\sin\nu\pi}P_\nu(-\cos\gamma). \tag{18}$$

Introducing $p^2 = -\nu(\nu+1)$, we obtain

$$\sum_{\ell=0}^{\infty}\frac{2\ell+1}{\ell(\ell+1)+p^2}P_\ell(\cos\gamma) = -\frac{\pi}{\sin\nu\pi}P_\nu(-\cos\gamma). \tag{19}$$

Comparing (16) and (19) shows we must extend the right-hand side sum of (16) to start at $\ell = 0$. The missing component $(1/4\pi p^2)$ is thus added and subtracted to complete the sum. We finally obtain the closed form expression of (12) as

$$\bar{c}_p(\gamma) = \frac{1}{4\sin\nu\pi}P_\nu(-\cos\gamma) - \frac{1}{4\pi\nu(\nu+1)}. \tag{20}$$

Substituting (20) into (12), we obtain

$$\nabla_s^2\bar{g}_p(\gamma) = \frac{1}{4\sin\nu\pi}P_\nu(-\cos\gamma) - \frac{1}{4\pi\nu(\nu+1)} \tag{21}$$

which we integrate twice and apply the requirement that $\bar{g}_p(\gamma)$ be finite everywhere and satisfy (9) to obtain (see Appendix A)

$$\bar{g}_p(\gamma) = \frac{\pi P_\nu(-\cos\gamma)}{\sin\nu\pi} - \log(1-\cos\gamma). \tag{22}$$

The presence of ν in the denominator in (21), however, means the solution is not valid for $p = 0$. Thus, for completeness we next consider the case when $p = 0$, that is,

$$\bar{c}_0(\gamma) = \frac{-1}{4\pi}\sum_{\ell=1}^{\infty}\frac{2\ell+1}{\ell(\ell+1)}P_\ell(\cos\gamma). \tag{23}$$

Parker (1994) examined the case of no tension ($p = 0$) and found the closed-form solution to be

$$\bar{g}_0(\gamma) = 2 - \frac{\pi^2}{6} + \text{dilog}\,[\sin^2(\gamma/2)], \tag{24}$$

where dilog is Euler's dilogarithm (e.g. Abramowitz & Stegun 1970), defined as

$$\text{dilog}(x) = \text{Li}_2(x) = -\int_0^x\frac{\log(1-t)}{t}\text{d}t = \sum_{k=1}^{\infty}\frac{x^k}{k^2}. \tag{25}$$

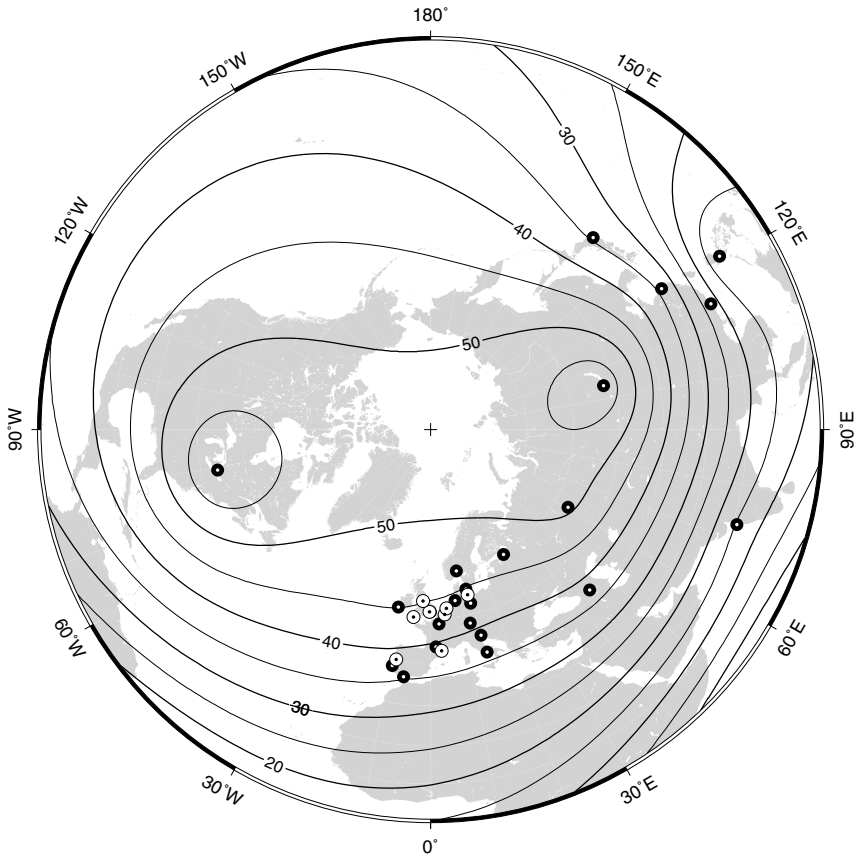

Figure 3. Contours (in μT) of the grid derived from our solution with moderate tension ($p = 10$). Note how this solution and the solid contours in Fig. 2 converge when approaching the data constraints.

The following identities are derived by Gradshteyn & Ryzhik (1980, eqs 8.926.1–2):

$$\sum_{\ell=1}^{\infty} \frac{1}{\ell} P_\ell(\cos\gamma) = -\log\left(\sin\frac{\gamma}{2}\right) - \log\left(1+\sin\frac{\gamma}{2}\right), \tag{26}$$

$$\sum_{\ell=1}^{\infty} \frac{1}{\ell+1} P_\ell(\cos\gamma) = \log\left(\frac{1+\sin\frac{\gamma}{2}}{\sin\frac{\gamma}{2}}\right) - 1. \tag{27}$$

Adding (26) and (27) and multiplying by $\frac{-1}{4\pi}$, we find

$$\bar{c}_0(\gamma) = \frac{1}{4\pi}\left[1 - \log\left(\frac{1+\sin\frac{\gamma}{2}}{\sin\frac{\gamma}{2}}\right) + \log\left(\sin\frac{\gamma}{2}\right) + \log\left(1+\sin\frac{\gamma}{2}\right)\right] \tag{28}$$

which simplifies to

$$\bar{c}_0(\gamma) = \frac{1}{4\pi}\left[1 + \log\sin^2\frac{\gamma}{2}\right]. \tag{29}$$

This solution matches the generalized Green's function for the Helmholtz operator given by Szmytkowski (2006). Again, integrating twice and requiring a finite solution as well as satisfying (9) results in (see Appendix A)

$$\bar{g}_0(\gamma) = -\frac{1}{4\pi}\mathrm{dilog}\left(\sin^2\frac{\gamma}{2}\right). \tag{30}$$

Comparison with Parker's (1994) solution (24) shows only a difference by a constant (which we represent by $\bar{z}$) and scale (included in the solution for α_j in 11).

2.1 The gradient of the Green's function

Following Sandwell (1987), we wish to use the interpolation scheme with measurements of both surface heights and directional gradients; we thus need to know the gradient $\nabla\bar{g}_p$. With $x = \cos\gamma$ we have

$$\nabla\bar{g}_p(\gamma) = \frac{\mathrm{d}\bar{g}_p(\gamma)}{\mathrm{d}\gamma}\hat{n} = \frac{\mathrm{d}\bar{g}_p(x)}{\mathrm{d}x}\frac{\mathrm{d}x}{\mathrm{d}\gamma}\hat{n}. \tag{31}$$

Evaluation of the derivatives is straightforward and with $\frac{\mathrm{d}x}{\mathrm{d}\gamma} = -\sin\gamma$ we obtain

$$\nabla\bar{g}_p(\gamma) = -\left\{\frac{\pi(\nu+1)}{\sin\nu\pi\,\sin\gamma}\left[\cos\gamma\,P_\nu(-\cos\gamma) + P_{\nu+1}\,(-\cos\gamma)\right] + \cot\left(\frac{\gamma}{2}\right)\right\}\hat{n}. \tag{32}$$

Here, $\hat{n}$ is the unit tangent vector along the arc between two points on the sphere.

2.2 The tension term

Given $p^2 = -\nu(\nu+1)$, the corresponding values for ν are

$$\nu = \frac{-1+\sqrt{1-4p^2}}{2}, \tag{33}$$

where only the positive root is needed on account of the relationship $P_\nu(x) = P_{1-\nu}(x)$. For the small range $0 \le p \le 1/2$ we find ν to be a real number between 0 and $-\frac{1}{2}$, but for larger values of p it becomes

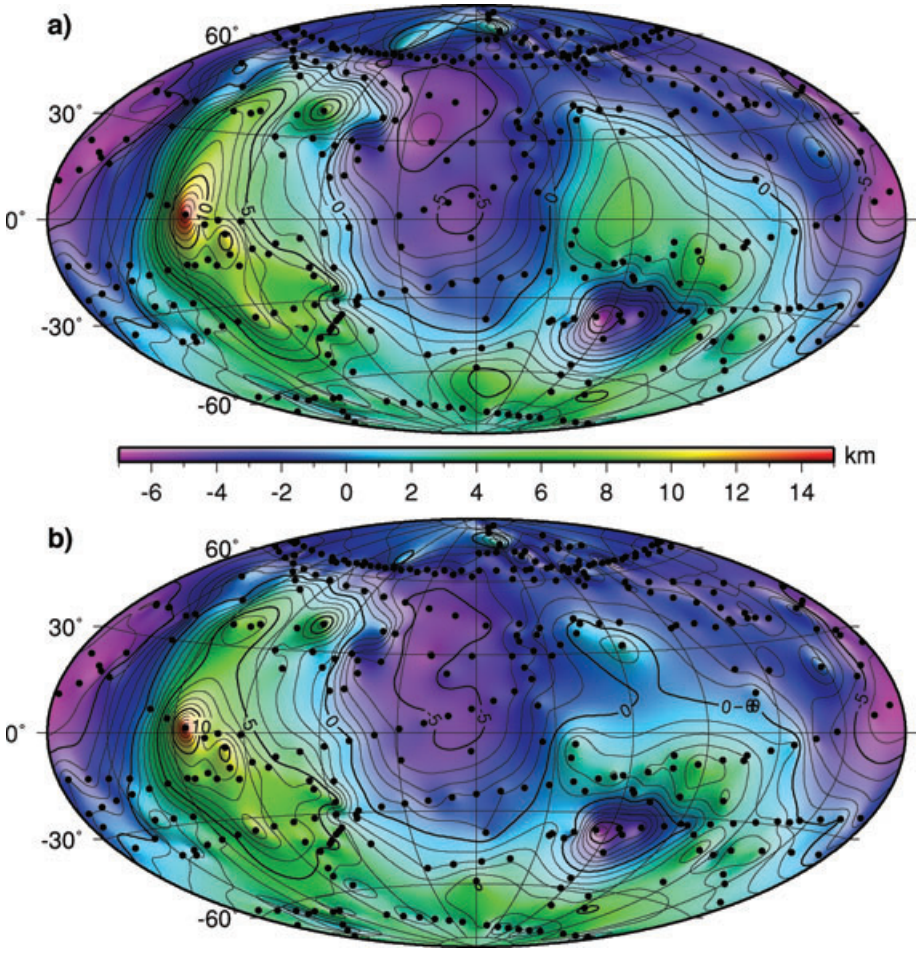

Figure 4. (a) Minimum curvature solution of Parker (1994) based on 370 measurements (solid circles) of the radius of Mars from Mariner 9 and Viking Orbiter spacecrafts (Smith & Zuber 1996). (b) Same calculation but with a tension factor of 20. In both cases the radii solutions are shown relative to a Mars ellipsoid with axes $a = 3399.472$, $b = 3394.329$ and $c = 3376.502$ km.

a complex number whose real part is $-\frac{1}{2}$. For these values the P_ν are called conical functions (e.g. Abramowitz & Stegun 1970).

2.3 Implementing the Green's function

While (22) is finite for all values of γ, the two competing log-like terms individually are singular when $\gamma \to 0$. We use approximations to P_ν from Spanier & Oldham (1987) that are accurate close to the singularity and find

$$\bar{g}_p(0) = \pi \cot \nu\pi - \log 2 + 2[E + \psi(1 + \nu)] \tag{34}$$

where $E = 0.57721\ldots$ is Euler's constant and $\psi(x)$ is the digamma function (e.g. Abramowitz & Stegun 1970). Although P_ν is not singular for $\gamma = \pi$, similar approximations can be used to obtain the special value

$$\bar{g}_p(\pi) = \frac{\pi}{\sin \nu\pi} - \log 2. \tag{35}$$

We have implemented the Green's function and its gradient in Matlab®; the source code is available from the authors upon request. Fig. 1 shows a family of Green's functions for a variety of tensions (including no tension). For comparison, all curves have been normalized. As is the case for Cartesian Green's functions for splines in tension (e.g. Wessel & Bercovici 1998), increasing the tension leads to a more localized weighting of data constraints as $\bar{g}_p(\gamma)$ then decreases more rapidly away from the origin. The same trend is even more apparent for the gradient. Our new Green's function (22) takes on a similar form to that of the 2-D Cartesian solution for a spline in tension given by

$$g(r) = \mathrm{K}_0(pr) + \log(pr), \tag{36}$$

where K_0 is the modified Bessel function of the second kind and order zero and r is the distance between two points (e.g. Mitášová & Mitáš 1993; Wessel & Bercovici 1998). In both cases the solution is a combination of two log-like terms whose singularities at $r = 0$ cancel. Numerically, our evaluation of P_ν is based on algorithms by Spanier & Oldham (1987). Close to $\gamma = 0, \pi$ these expressions converge very slowly. Thus, until a rapid approximation is developed it likely is faster to pre-calculate (22) for a dense set of arguments and then interpolate when values at other angles are required.

3 DISCUSSION

Parker (1994) demonstrated spherical gridding with his dilogarithm solution on a small data set of magnetic field measurements obtained from 25 observatories from the year 1900 (his table 2.07B). We are

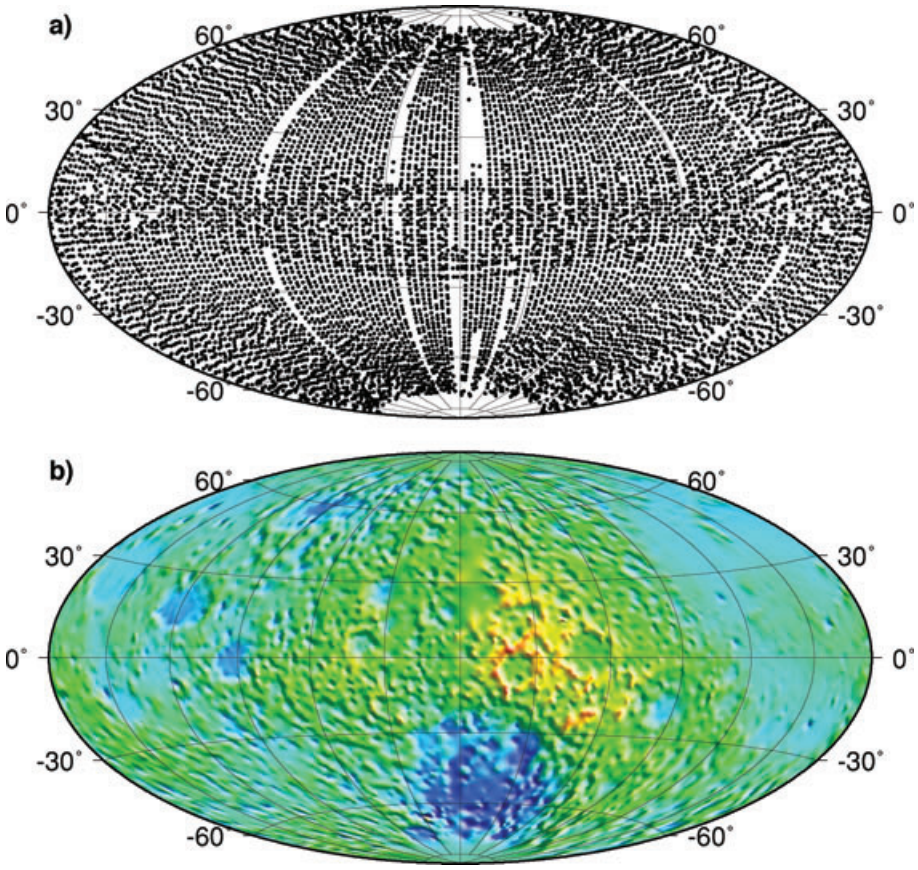

Figure 5. (a) Distribution of a subset of lidar measurements from the Clementine mission to the Moon (Smith *et al.* 1997). (b) Our 15 × 15 arcmin interpolation using a tension of 25.

able to reproduce his findings in general (Fig. 2), but since his table contained the wrong longitude for one of the constraining stations (Oslo, with a correct longitude of 10.45E, not the reported 104.5E) the contours are necessarily somewhat different near these two locations.

We also present a calculation for moderate ($p = 10$) tension in Fig. 3. Note that the two solutions are considerably different far away from the constraining data points but converge near these points. Parker (1994) also showed the spline misfit at 8 additional locations (his table 2.07C) not included in determining the spline coefficients. We searched for the value of tension that would minimize the misfit variance at those stations. For $p = 38.9$ we minimized the misfit, yielding a variance reduction of almost 40 per cent relative to Parker's (1994) solution with no tension. This variance reduction results from the further attenuation of unnecessary undulations typical of minimum curvature splines. Of course, the measurements we used here can also be considered as the radial components of a vector field that satisfies the differential equations describing the physics of the magnetic field. Thus, another option is to develop an interpolator that takes into account the constraints imposed by these equations (e.g. Shure *et al.* 1982).

Next, we demonstrate our solutions for a modest data set of 370 occultation measurements of the radius of Mars, thus reproducing part of the analysis of Smith & Zuber (1996). Fig. 4(a) displays the minimum curvature solution (i.e. no tension) while Fig. 4(b) shows how a tension of $p = 20$ modifies the surface. The solid dots indicate the sparse data distribution. The two solutions agree well near the observations but the minimum curvature solution tends to produce broader local maxima and minima away from data.

Finally, we examine how our method handles a much larger data set. We use a decimated set of lidar measurements from the Clementine mission, yielding 10082 individual Lunar topographic heights relative to a uniform sphere of radius 1738 km (Smith *et al.* 1997). The point distribution is displayed in Fig. 5 (top panel), while our solution, evaluated on a uniform 15 × 15 arcmin grid, is presented below. This calculation involved the solution of a 10082^2 linear system which took about 1 hour on our workstation. Thus, fairly large data sets may be accommodated but will require considerable computer memory and perhaps 64-bit addressing. However, as the data density increases, gridding becomes more localized and almost any interpolation method will yield acceptable solutions.

Because of the spherical treatment, our Green's function is most useful for truly global data (or at least data that cover a significant part of the Earth or other spherical bodies such as our last two examples). More localized data sets may be gridded instead by Cartesian methods after a suitable map projection has been applied. Moreover, given the N by N matrix that must be inverted, only moderate data sets ($N < 10\,000$ points) can be used directly on most computers. It is possible to break down large data sets into smaller, overlapping subsets and grid these separately, then blend the solutions into a final result. However, in this paper we have simply chosen to present the new Green's function and demonstrate its use for simple spherical gridding.

ACKNOWLEDGMENTS

This work was supported by grant OCE-0452126 from the National Science Foundation to P.W. We thank John Goff, Jun Korenaga and one anonymous reviewer whose comments lead to improvements in the manuscript. Greg Neumann kindly provided the planetary data used in Figs 4 and 5. This is SOEST contribution no. 7459.

REFERENCES

Abramowitz, M. & Stegun, I., 1970. *Handbook of Mathematical Functions,* 1046 pp., Dover, New York.

Arfken, G.B. & Weber, H.J., 1995. *Mathematical Methods for Physicists,* 4th edn, 1029 pp., Academic Press, New York.

Briggs, I.C., 1974. Machine contouring using minimum curvature, *Geophysics*, **39,** 39–48.

Courant, R. & Hilbert, D., 1953. *Methods of Mathematical Physics,* Vol. 1, 561 pp., Interscience, New York, NY.

Duffy, D.G., 2001. *Green's Functions with Applications,* 443 pp., Chapman and Hall/CRC, Boca Raton, FL.

Freeden, W., 1984. Spherical spline interpolation—basic theory and computational aspects, *J. Comput. Appl. Math.*, **11,** 367–375.

Gradshteyn, I.S. & Ryzhik, I.M., 1980. *Table of Integrals, Series, and Products,* 5th edn, 1204 pp., Academic Press, San Diego, CA.

Greenberg, M.D., 1971. *Applications of Green's Functions in Science and Engineering,* 141 pp., Prentice-Hall, Englewood Cliffs, NJ.

Inoue, H., 1986. A least-squares smooth fitting for irregularly spaced data: finite-element approach using the cubic B-spline basis, *Geophysics*, **51,** 2051–2066.

Menke, W., 1991. Applications of the POCS inversion method to interpolating topography and other geophysical fields, *Geophys. Res. Lett.*, **18,** 435–438.

Mitášová, H. & L. Mitáš, 1993. Interpolation by regularized spline with tension: I. Theory and implementation, *Math. Geol.*, **25,** 641–655.

Olea, R.A., 1974. Optimal contour mapping using universal kriging, *J. geophys. Res.*, **79,** 696–702.

Omre, H. & Halvorsen, K.B., 1989. The Bayesian bridge between simple and universal kriging, *Math. Geol.*, **21,** 767–786.

Parker, R.L., 1994. *Geophysical Inverse Theory,* 1st edn, 386 pp., Princeton Univ. Press, Princeton, New Jersey.

Reguzzoni, M., Sanso, F. & Venuti, G., 2005. The theory of general kriging, with applications to the determination of a local geoid, *Geophys. J. Int.*, **162,** 303–314.

Renka, R.J., 1984. Interpolation on the surface of a sphere, *ACM Trans. Math. Software*, **10,** 437–439.

Renka, R.J., 1997. SSRFPACK: interpolation of scattered data on the surface of a sphere with a surface under tension, *ACM Trans. Math. Software*, **23,** 435–442.

Roach, G.F., 1982. *Green's Functions,* 2nd edn, 344 pp., Cambridge University Press, Cambridge, UK.

Sandwell, D.T., 1987. Biharmonic spline interpolation of Geos-3 and Seasat altimeter data, *Geophys. Res. Lett.*, **14,** 139–142.

Smith, W.H.F. & Wessel, P., 1990. Gridding with continuous curvature splines in tension, *Geophysics*, **55,** 293–305.

Smith, D.E. & Zuber, M.T., 1996. The shape of Mars and the topographic signature of the hemispheric dichotomy, *Science*, **271,** 184–187.

Smith, D.E., Zuber, M.T., Neumann, G. & Lemoine, F., 1997. Topography of the Moon from the Clementine lidar, *J. geophys. Res.*, **102,** 1591–1611.

Shure, L., Parker, R.L. & Backus, G.E., 1982. Harmonic splines for geomagnetic modelling, *Phys. Earth planet. Int.*, **28,** 215–229.

Spanier, J. & Oldham, K.B., 1987. *An Atlas of Functions,* 1st edn, 700 pp., Hemisphere Publ. Corp., Washington, DC.

Swain, C.J., 1976. A FORTRAN IV program for interpolating irregularly spaced data using the difference equations for minimum curvature, *Comput. & Geosci.*, **1,** 231–240.

Szmytkowski, R., 2006. Closed form of the generalized Green's function for the Helmholtz operator on the two-dimensional unit sphere, *J. Math. Phys.*, **47**(063506), 1–11.

Wahba, G., 1990. *Spline Models for Observational Data,* 169 pp., Society for Industrial and Applied Mathematics, Philadelphia, PA.

Wegman, E.J. & Wright, I.W., 1983. Splines in statistics, *J. Am. Stat. Assn.*, **78,** 351–365.

Wessel, P. & Bercovici, D., 1998. Interpolation with splines in tension: a Green's function approach, *Math. Geol.*, **30,** 77–93.

APPENDIX A: THE GENERALIZED GREEN'S FUNCTION

To arrive at the closed form solution for $\bar{g}_p(\gamma)$, we integrate (21) in the limit of spherical isotropy, that is,

$$\frac{1}{\sin\gamma}\frac{\mathrm{d}}{\mathrm{d}\gamma}\left[\sin\gamma\,\frac{\mathrm{d}\bar{g}_p(\gamma)}{\mathrm{d}\gamma}\right] = \frac{1}{4\sin\nu\pi}P_\nu(-\cos\gamma) - \frac{1}{4\pi\nu(\nu+1)}. \tag{A1}$$

While this integration is straightforward, we provide the details here for completeness. The first integral

$$\sin\gamma\,\frac{\mathrm{d}\bar{g}_p(\gamma)}{\mathrm{d}\gamma} = \int^{\gamma}\sin\gamma'\left[\frac{P_\nu(-\cos\gamma')}{4\sin\nu\pi} - \frac{1}{4\pi\nu(\nu+1)}\right]\mathrm{d}\gamma' \tag{A2}$$

may be simplified as follows. Since $P_\nu(x)$ satisfies Legendre's equation it is straightforward to show that

$$(1-x^2)\frac{\mathrm{d}P_\nu(x)}{\mathrm{d}x} = -\nu(\nu+1)\int^{x}P_\nu(\xi)\,\mathrm{d}\xi. \tag{A3}$$

We next make the variable transformation $x = -\cos\gamma$ in (A3) hence (A2) becomes

$$\sin\gamma\,\frac{\mathrm{d}\bar{g}_p}{\mathrm{d}\gamma} = -\frac{1}{4\pi\nu(\nu+1)}\left[\frac{\pi\sin\gamma}{\sin\nu\pi}\frac{\mathrm{d}P_\nu(-\cos\gamma)}{\mathrm{d}\gamma} - \cos\gamma + a\right], \tag{A4}$$

where a is a constant of integration. The integral of (A4) results in

$$\bar{g}_p(\gamma) = -\frac{1}{4\pi\nu(\nu+1)}\left\{\frac{\pi P_\nu(-\cos\gamma)}{\sin\nu\pi} - \log(\sin\gamma) + a\log\left[\tan\left(\frac{\gamma}{2}\right)\right]\right\} + b, \tag{A5}$$

where b is a second constant of integration. Since both $P_\nu(-\cos\gamma)$ and $\log(\sin\gamma)$ are singular at $\gamma = 0$ whereas the last logarithmic term is singular for $\gamma = 0,\ \pi$, we must ensure all singularities cancel by fixing a. The singular behavior of $P_\nu(-\cos\gamma)$ is (Spanier & Oldham 1987)

$$\lim_{\gamma\to 0}P_\nu(-\cos\gamma) \sim \frac{\sin\nu\pi}{\pi}\log\left(\frac{1-\cos\gamma}{2}\right). \tag{A6}$$

Hence, the logarithmic terms within the braces in (A5) must satisfy

$$\lim_{\gamma\to 0}\left[\log\left(\frac{1-\cos\gamma}{2}\right) - \log(\sin\gamma) + a\log\left(\frac{1-\cos\gamma}{\sin\gamma}\right)\right] = 0. \tag{A7}$$

The choice $a = -1$ thus ensures $\bar{g}_p(\gamma)$ is finite. To satisfy the orthogonality condition (9), we set $b = 0$ and, after contracting the logarithmic terms and using $p^2 = -\nu\,(\nu+1)$, obtain

$$\bar{g}_p(\gamma) = \frac{1}{4\pi p^2}\left[\frac{\pi P_\nu(-\cos\gamma)}{\sin\nu\pi} - \log(1-\cos\gamma)\right]. \tag{A8}$$

As a practical matter, the leading factor may be absorbed into the solution for the spline coefficients α_j, hence the simplified final solution is given by (22).

For the case $p = 0$ we substitute (29) in (12) to obtain

$$\frac{1}{\sin\gamma}\frac{\mathrm{d}}{\mathrm{d}\gamma}\left[\sin\gamma\frac{\mathrm{d}\bar{g}_0(\gamma)}{\mathrm{d}\gamma}\right] = \frac{1}{4\pi}\left(1 + \log\sin^2\frac{\gamma}{2}\right), \tag{A9}$$

with the first integral

$$\sin\gamma\frac{\mathrm{d}\bar{g}_0(\gamma)}{\mathrm{d}\gamma} = \frac{1}{4\pi}\left[\int^{\gamma}\left(\sin\gamma'\log\sin^2\frac{\gamma'}{2} + \sin\gamma'\right)\mathrm{d}\gamma'\right]. \tag{A10}$$

Using the variable transformation $x' = \frac{1-\cos\gamma'}{2}$ in (A10) we obtain

$$\sin\gamma\frac{\mathrm{d}\bar{g}_0(\gamma)}{\mathrm{d}\gamma} = \frac{1}{4\pi}\left[(1-\cos\gamma)\log\left(\frac{1-\cos\gamma}{2}\right) + a - 1\right] \tag{A11}$$

and introduce the change of variable $u' = \frac{1+\cos\gamma'}{2}$ in (A11) to obtain

$$\bar{g}_0(\gamma) = \frac{1}{4\pi}\left[\int^{u}\frac{\log(1-u')}{u'}\mathrm{d}u' + (a-1)\log\tan\frac{\gamma}{2} + b\right]. \tag{A12}$$

To eliminate all singularities in $\bar{g}_0(\gamma)$ we choose $a = 1$ and to satisfy (9) we set $b = 0$. The remaining integral matches the definition of Euler's dilogarithm (25) resulting in (30).